Utilizing a novel green ternary polymeric nanocomposite material to remove tetracycline antibiotic effectively from aqueous solutions

Nazir Mustapha[1] · Marwa H. Gouda[2] · M. Abdel Rafea[1] · M. Salerno[3] · Ashour M. Ahmed[1,4] · Noha A. Elessawy[5]

Abstract

Highly efficient removal of tetracycline antibiotic residue from aqueous solution was demonstrated by a novel, cost effective and environmentally friendly adsorbent consisting in composite polymeric beads of sodium alginate, chitosan and polyvinyl pyrrolidone, doped with equal ratio of sulfonated graphene oxide and sulfonated titania, fabricated via simple blending method using calcium chloride as a crosslinker. The adsorption parameters of beads amount, initial tetracycline concentration, adsorption time and solution pH were investigated. Furthermore, adsorption time, beads amount, and the initial tetracycline concentration were optimized using the response surface methodology model. Pseudo-second-order kinetic equation was fitted to the adsorption process' kinetics. It was discovered that the electrostatic attraction and hydrogen bonding, which primarily contribute to the noticeably enhanced adsorption ability, are the essential factors driving the adsorption mechanism. The maximum antibiotic adsorption capacity of the nanocomposite beads reached 357 mg/g.

Keywords Sodium alginate · Upcycling plastic waste · Sulfated graphene oxide · Sulfated titanium oxide · Tetracycline removal · Adsorption

1 Introduction

Tetracycline (TC) is a type of polycyclic compound with antimicrobial properties. This common antibiotic ranks second in usage and production worldwide, is widely used in agriculture and animal husbandry and is largely present in soil and aquatic environment [1–5]. It has been proved that TC causes bacteria resistance and leads to ecological damage, so that its removal from soil or aquatic environment is important for human health. Different methods including advanced oxidation, chemical coagulation, membrane separation, adsorption and biodegradation were used to remove TC from aqueous solution. Among these methods, the adsorption one was used most extensively in TC removal from wastewater because of its high efficiency and simplicity [6–8].

Recently, the use of biopolymers such as sodium alginate (SA) for designing natural adsorbents has gained attention due to safety and cost concerns [9, 10]. SA beads are used in various water treatment applications [11], but this practice has been hindered because of the weak mechanical properties and easy disintegration of the beads [9, 11, 12]. To overcome this issue, Luo et al. used modified alginate beads by polymers blending to fabricate multi-components matrix that allowed enhancement of adsorbent porosity and functional groups with desirable properties to remove TC from aqueous solutions more effectively [13]. Indeed, natural polymers are available for blending with SA such as chitosan, which is a sustainable and environment friendly polymer, in line with the green chemistry principle of modern

✉ Noha A. Elessawy
   nony_essawy@yahoo.com

1   Department of Physics, College of Science, Imam Mohammad Ibn Saud Islamic University (IMSIU), Riyadh 11623, Kingdom of Saudi Arabia

2   Polymer Materials Research Department, Advanced Technology and New Materials Research Institute (ATNMRI), City of Scientific Research and Technological Applications (SRTA-City), Alexandria 21934, Egypt

3   Department of Physics, IGDORE, University of Genova, Genova 16146, Italy

4   Physics Department, Faculty of Science, Beni-Suef University, Beni-Suef 62514, Egypt

5   Computer Based Engineering Applications Dept., Informatics Research Institute IRI, City of Scientific Research & Technological Applications (SRTA-City), Alexandria 21934, Egypt

science [14]. Consequently, Erdem et al. synthesized halloysite nanotube-based composites from chitosan and alginate biopolymers to remove TC effectively from aqueous solutions [15].

The current trend of new adsorbents goes in the direction of polymers blending and polymer functionalization with the incorporation of nanomaterials in the polymer matrix to increase the removal efficiency [16]. For example, titania (TiO_2) nanotubes have been demonstrated as an effective photocatalyst for organic contaminates degradation [17, 18]. It has been demonstrated that photocatalytic degradation of TC on TiO_2 surface is a promising treatment for TC contaminated effluent [19, 20]. Furthermore, using of sulfonated titanium oxide nanotubes (S-TiO_2) is expected to have a good adsorption affinity for antibiotics by electrostatic attraction between sulfate groups of S-TiO_2 and amine groups of the antibiotics. Sulfonated graphene oxide (SGO) is a graphene functionalized with sulfonic group that has abundant different groups containing oxygen (e.g., -OH,-COOH, SO_3H_2), with good water dispersibility [21, 22], which made it an excellent adsorbent for pharmaceutical residue removal via the combination of $\pi - \pi$ stacking, electrostatic attraction and hydrogen bonds interaction between its oxygenated functional groups and contaminates molecules [19, 20, 23–25]. Thanks to its excellent properties, SGO has already been used as an effective adsorbent for different organic pollutants in aqueous solutions [21, 22]. Therefore, in our study SGO was mixed with S-TiO_2 to form a novel nanocomposite.

In particular, the separation and recycling of the nanoadsorbent during the water treatment is a big challenge in the adsorption process, which we address by incorporating the adsorbent nanomaterial in a polymeric matrix having high adsorption properties thanks to its porosity and to abundant functional groups on the surface. To achieve this, we prepared and characterized SGO_STiO$_2$@SA/CS/PVP nanocomposites beads as an adsorbent for organic pollutants. In addition, SGO was obtained from waste plastic by recycling technology as a green option. The effectiveness of the prepared nanocomposite for adsorption of TC antibiotic was investigated. In order to minimize the number of experiments, investigate the correlations between the response and the effective dependent variables, and ascertain the ideal process operating parameters, the response surface methodology (RSM) was employed as a statistical design. Our goal is the final nanoengineered adsorbent to be a viable option for a variety of industrial uses, the most important being the secure removal of dangerous contaminants from the environment.

2 Materials and methods

2.1 Materials

Sodium alginate (SA) extracted from red algae (medium MW), chitosan (CS) with degree of acetylation 85% (medium MW), polyvinyl pyrrolidone (PVP) with average MW 29,000 g/mol, sodium hydroxide, calcium chloride and titania titanium (IV) dioxide rutile type (powder, $TiO_2 \leq 5$ mm) and acetic acid 99.5% purity were bought from sigma Aldrich.

2.2 Preparation of nanocomposite beads

SA, CS and PVP polymers were dissolved separately as following: 3 g of SA in deionized (DI) water at 50 °C, 0.5 g of CS in 50 mL DI water at 50 °C with 1 mL acetic acid, 1 g of PVP in 10 mL DI water at room temperature (RT). Then all polymer solutions were mixed for 4 h at RT.

According to our previous studies, the synthesized S-TiO_2 nanotubes [26] and SGO [21] were mixed in a 1:1 wt ratio with few drops of DI water and sonicated for 1 h to form a homogenous nanocomposite mixture before adding the polymers blend. Then the SGO_STiO$_2$@SA/CS/PVP solution was stirred for 6 h. The polymeric nanocomposite mixture was injected in a plastic syringe and dropped slowly in a solution containing 6 wt% $CaCl_2$ (6 gm in 100 mL water) which alkalined with 4 wt% NaOH (4 gm in 100 mL water). As a result the SGO_STiO$_2$@SA/CS/PVP solution crosslinked and formed beads. The beads were left in the crosslinking solution overnight before being repeatedly washed with DI water and then dried at 50 °C for 6 h.

2.3 Characterization of SGO, S-TiO_2 and nanocomposite beads

Some basic characterization of the prepared SGO, S-TiO_2 powder and SGO_STiO$_2$@SA/CS/PVP nanocomposite beads were conducted, including surface functional groups analysis using Fourier-transform infrared (FTIR) spectroscopy (Shimadzu FTIR-8400 S, Japan). The morphology of the nanocomposite beads was characterized with scanning electron microscopy (SEM, JEOL JSM/6360LA, Japan) and the morphology of SGO and S-TiO_2 was characterized with transmission electron microscopy (TEM, TECNAI G20, the Netherlands). The crystallographic phases of SGO and S-TiO_2 particles and SGO_STiO$_2$@SA/ IC/PVP beads were obtained using X-ray diffraction (XRD, Schimadzu 7000, Japan). Zeta potential measurements were performed for SGO, S-TiO_2 and SGO_STiO$_2$@SA/CS/PVP nanocomposite beads using Zetasizer Nano ZS90 Size Analyzer (Malvern Panalytical, UK).

2.4 Evaluation of antimicrobial properties of nanocomposite beads

To assess the efficacy of the fabricated nanocomposite films, various pathogens were used as antimicrobial models such as *Bacillus subtilis* (Gram-positive bacteria), *E. coli* (Gram-negative bacteria), *Aspergillus fumigatus* (fungus) and *Candida albicans* (yeast). Initially, each type of microorganism was injected into the liquid medium at 220 rpm and 37 °C until the optical density (OD) at 600 nm grew up to 0.6. The microbial solution was diluted at a 1:1000 vol ratio. 0.01 g of sterilized SGO_STiO$_2$@SA/CS/PVP nanocomposite beads were added to 3 mL of microbial solution and kept at 220 rpm and 37 °C for 24 h. We then measured the OD and calculated the inhibition coefficient I as follows:

$$I\,(\%) = \frac{OD_{\text{control sample}} - OD_{\text{treated sample}}}{OD_{\text{control sample}}} \times 100 \tag{1}$$

2.5 Adsorption tests

A batch equilibration method was used to conduct the adsorption experiments. A range of TC antibiotic concentrations (25, 50, 75, and 100 mg/L) were used by dilution of stock solutions containing 1 g/L of TC. The pH of the solutions was changed using 0.1 M NaOH and 0.1 M HCl. Using UV-visible spectroscopy, the concentrations of TC in the solution were measured at wavelengths of 610 nm. The adsorbed amounts were calculated using the following equations:

$$q_t = \frac{C_0 - C_t}{m}V \tag{2}$$

$$q_e = \frac{C_0 - C_e}{m}V \tag{3}$$

where q_t and q_e (mg/g) are the mass of TC adsorbed per unit mass of the nanocomposite film at generic time and equilibrium, respectively; C_0, C_t, and C_e (mg/L) are the TC concentrations at initial, generic and equilibrium time, respectively. V (L) is the volume of TC solution; m (g) is the mass of nanocomposite film. We obtained the removal efficiency R from this formula:

Table 1 Independent variable levels that are coded in RSM experimental design

Symbol	Independent variable	Coded levels		
		-1	0	1
A	time / min	60	90	120
B	initial concentration / mg/L	25	50	75
C	adsorbent dose / mg	5	10	15

$$R\,(\%) = \frac{C_0 - C_t}{C_0} \times 100 \tag{4}$$

The pH was set at 6 and the adsorption period was varied within a range of 5 to 120 min for kinetics and isotherm studies as illustrated in Supplementary information.

2.6 Optimization of the adsorption

To optimize adsorption, we investigated the possible correlation between factors and responses using RSM. The matrix with 17 trials was selected following Box–Behnken design [27, 28]. Three factors were used: A (time, in min), B (initial concentration, in mg/L) and C (adsorbent dose, in mg), and three levels described as − 1, 0, and 1, as illustrated in Table 1. We used the software Design-Expert 13.0.9.0 from Stat-Ease Inc. (MN, USA). The established models were assessed statistically by analysis of variance (ANOVA) using the F-test for determination of significance. The R^2 determination coefficient can be seen as a figure of merit describing the quality of the results [29].

2.7 Regeneration and recycling

To evaluate the ability of the nanocomposite beads to regenerate, 50 mg of SGO_STiO$_2$@SA/CS/PVP nanocomposite beads was added to conical flask contains 25 mL of 50 mg/L of TC solution. For two hours, the solution was agitated at 150 rpm. Following adsorption, the nanocomposite beads underwent filtration separation, 30 min of ultrasonication with a solution containing 10 mL of 0.1 M NaOH and 100 mL of ethanol, filtering, washing, drying at 60 °C for 4 h, and reuse. After that, the filter fluid's concentration was determined, and the preceding steps were carried out five times.

3 Results and discussion

3.1 Characterization of SGO, STiO$_2$ and nanocomposite beads

In Fig. 1a the FTIR spectra of SGO, S-TiO$_2$ and composite beads show all the respective functional groups. The SGO_STiO$_2$@SA/CS/PVP beads in the top-most panel show a broad band at 3200–3600 cm^{-1} that refers to OH groups of SA, CS and SGO, while the peak close to 2178 cm^{-1} is assigned to (C-N) bond of PVP [18] and the peak at 1580 cm^{-1} is referred to NH$_2$ groups of CS [28]. The peak at 1419 cm^{-1} corresponds to COO group of SA and SGO. The peaks around 1050 and 1150 cm^{-1} are referred to sulfonic groups of SGO and S-TiO$_2$; additionally, the peak at

Fig. 1 (**a**) FTIR spectra, (**b**) XRD patterns, (**c-d**) TEM images for (**c**) SGO and (**d**) S-TiO$_2$, (**e**) SEM image and (**f**) zeta potentials of SGO_STiO$_2$@SA/CS/PVP nanocomposite beads
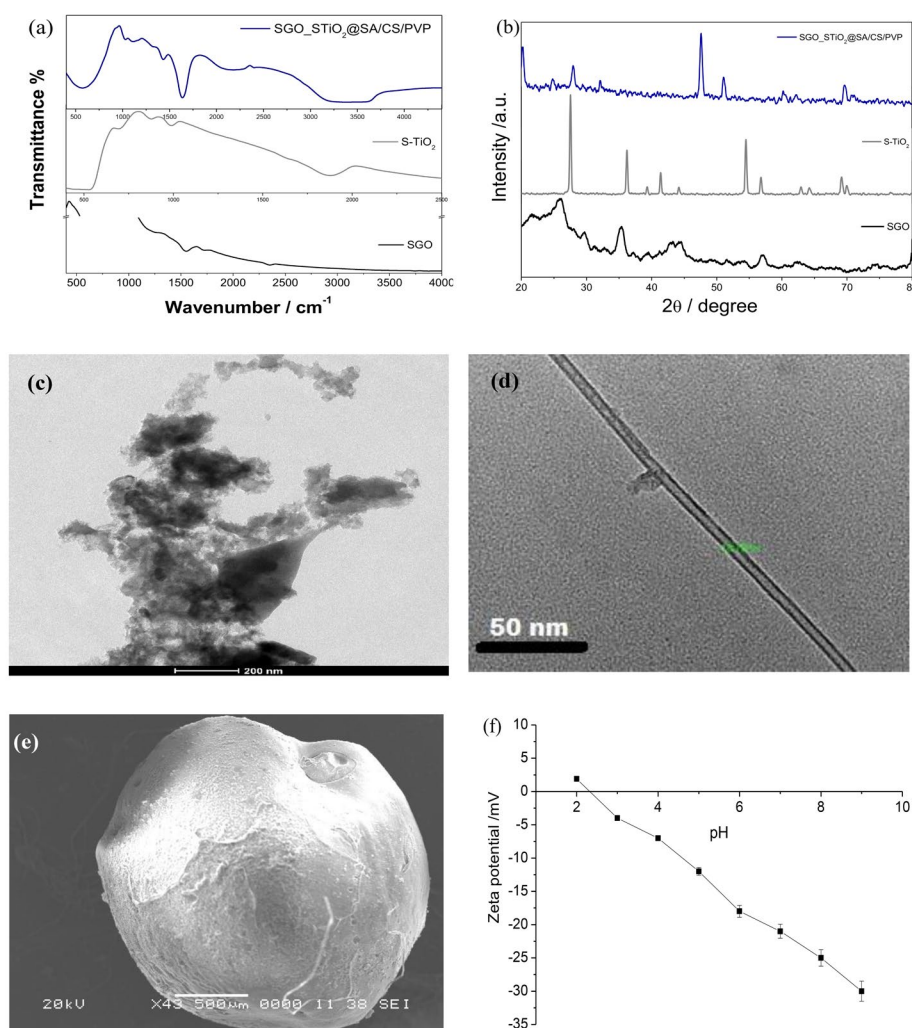
715 cm^{-1} confirms the presence of TiO$_2$ in the beads [26]. For the S-TiO$_2$ nanotubes (middle-panel in Fig. 1a), the Ti-O bonds appeared at 715 and 985 cm^{-1} and the broad peak at 1850 cm^{-1} is referred to O-H bonds as a result of moisture adsorption on S-TiO$_2$ hydrophilic surface, while the peak at 900 cm^{-1} corresponds to sulfate ion coordinated to Ti$^+$ metal cation. For SGO (bottom-most panel) the shoulders at 1284 and 1750 cm^{-1} can be attributed to epoxy and C=O of carboxylic acid groups [22] while the sulfonic groups are shown at 1550 cm^{-1}.

In Fig. 1b, all the XRD patterns of the different materials are shown. In the bottom-most plot, SGO shows the sulfonation of GO whereas a broad peak emerges at 2θ position of 26°, showing partial GO sheets restacking by π-π interactions [30]. In S-TiO$_2$ (middle-panel) the typical XRD peaks of S-TiO$_2$ and TiO$_2$ appear at 28°,36°,41° and 54°, where incorporation of sulfate groups to TiO$_2$ just reduced the intensity of the peaks as a result of change in rutile crystalline phase [31]. Finally, in the polymeric nanocomposite beads

SGO_STiO$_2$@SA/CS/PVP (top-most panel of Fig. 1b) the amorphous structure of polymers can be observed, where the peaks of SGO and S-TiO$_2$ exhibit reduced intensity as a result of the dominating amorphous polymer structure.

The TEM images in Fig. 1c reveal the morphological structure of the different nanomaterials in the composite: in Fig. 1d a representative S-TiO$_2$ nanotube is shown, with ~12 nm diameter and ~400 nm length; on other hand, in Fig. 1c SGO appears as a micro sheet with thickness in the nano size scale, and the dark spots are the sulfonic functional groups. In Fig. 1e, a typical SEM image of a polymeric nanocomposite bead is finally presented, exhibiting globular, quasi-spherical shape in the micrometer size scale.

Figure 1f reports the zeta potentials of the SGO_STiO$_2$@SA/CS/PVP nanocomposite beads. It was noted that when pH increased from 3 to 9, the zeta potential diminished as the beads surface was highly oxidized with many oxygen functionalities such as sulfonic, carboxylic and hydroxyl

groups. This behavior makes them appropriate for adsorption of organic cations in different environmental pH [32].

3.2 Antimicrobial activities

The results of the antimicrobial activity tests of SGO_STiO$_2$@SA/CS/PVP nanocomposite are presented in Fig. 2. After 24 h of contact between the evaluated nanocomposite beads and the inoculum of *E. coli*, *Bacillus subtilis*, *Aspergillus fumigatus*, and *Candida albicans*, the inhibition coefficient relative to the control sample was recorded. Obviously the beads had good antibacterial and antifungal effect, reaching inhibition levels always above 60% for all considered strains and in particular as high as 81% for *E. Coli* and even 89% for *Bacillus subtilis*. This score may be ascribed to the antimicrobial properties of SGO and S-TiO$_2$ [33–35].

3.3 Adsorption batch experiments

Since pH strongly affects the charge of the adsorbent surface functional groups (Fig. 3a), it is important to know what pH is best for improving the TC adsorption. The effect of solution pH on adsorption process by the SGO_STiO$_2$@SA/CS/PVP nanocomposite was characterized and the results are shown in Fig. 3b. As previously mentioned and already observed in Fig. 1f, the surface of SGO_STiO$_2$@SA/CS/PVP nanocomposite beads contains many negatively charged groups, which makes it appropriate for adsorption of organic cations. Additionally, in order to find the best pH value during effective operation of the beads in TC removal,

we investigated the influence of solution pH on adsorption of TC onto prepared nanocomposite beads between 2 and 9. It was observed that the removal efficiency improved for an increase of pH between 2 and 6. Such a finding has been compared with a model of the surface chemistry of the beads, as shown in Fig. 3c. Actually, TC has amphoteric characteristic [36], such that its molecules are both negative and positive at pH between 3 and 7. However, at low pH values, around the bead there are many hydronium ions in competition with the cations of TC. Although an electrostatic repulsion exists at pH less than 5, removal efficiency was comparatively high, which may be ascribed to the hydrogen bonding and $\pi-\pi$ electron donor$-$acceptor interaction between the surface of SGO_STiO2@SA/CS/PVP beads and the TC molecules. This can be compared with the FTIR results. However, in the TC molecules the functional groups - hydroxyl, phenol, amine, and enone moieties - formed hydrogen bonds with the sulfate, carboxyl and hydroxyl functional groups on the beads. Meanwhile, by increasing the solution pH up to 6, the hydroxyl and carboxylic groups of the nanocomposite film are increasingly ionized so that the electrostatic attraction between TC cations and bead surface increases, giving rise to enhancement of removal efficiency. Conversely, as the solution pH increases from 7 to 9, the TC adsorption decreases because of a rise in the electrostatic repulsion between the TC anions and the negatively charged bead surface. Therefore, a solution pH of 6 was selected as the best value for TC removal during the subsequent experiments.

Next, a batch adsorption process at solution pH of 6 and operating time of 120 min was conducted to evaluate

Fig. 2 Antimicrobial assessment for SGO_STiO$_2$@SA/CS/PVP nanocomposite beads versus the different micro-organism models considered
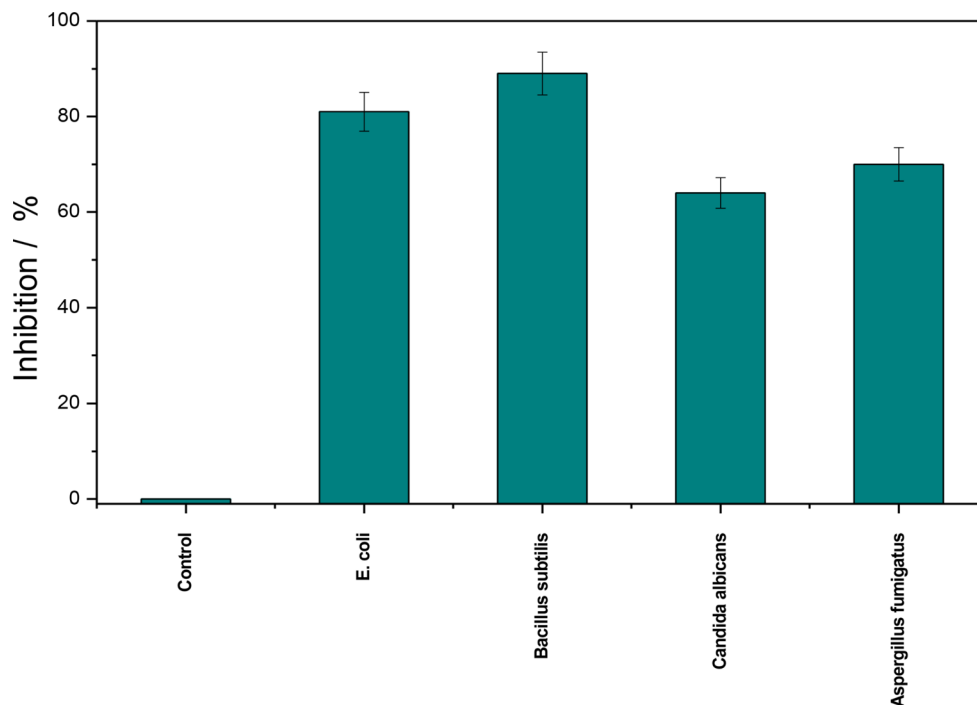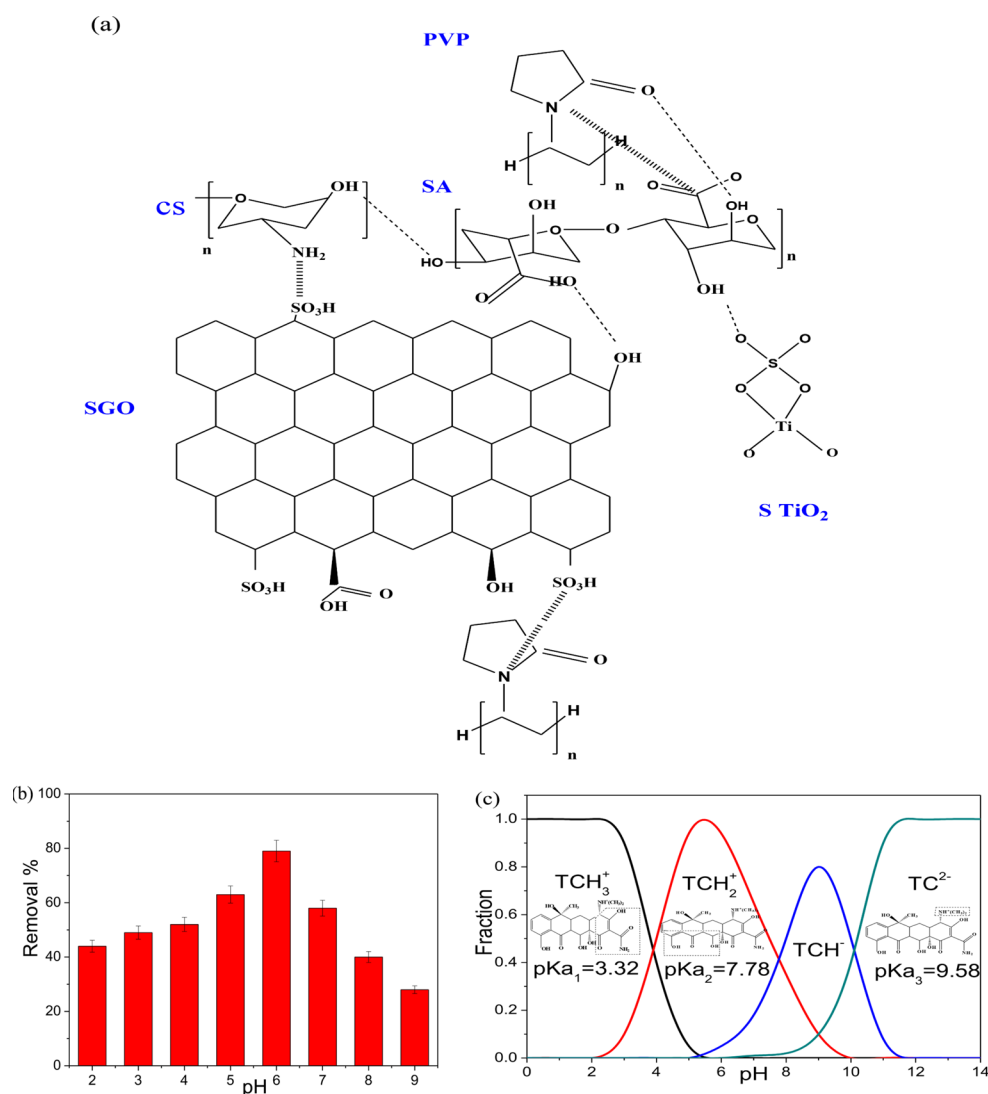
Fig. 3 (**a**) suggested structure of SGO_STiO$_2$@SA/CS/PVP nanocomposite beads (**b**) effect of solution pH on TC removal by SGO_STiO$_2$@SA/CS/PVP nanocomposite beads (at 50 mg/L initial concentration, 0.2 mg/mL adsorbent dose, 25℃, 120 min), (**c**) structure and surface speciation of TC that is pH dependent

the adsorption of SGO_STiO$_2$@SA/CS/PVP nanocomposite beads, whose results are presented in Fig. 4a. Over the time, the adsorption capacity increased with progressively decreasing slope, apparently achieving equilibrium after about 100 min. This can be explained by the fact that a balance between the adsorption and desorption of TC molecules occurs after a certain amount of time, making the remaining empty surface sites harder to employ.

In Fig. 4b, the antimicrobial activity tests of SGO_STiO$_2$@SA/CS/PVP nanocomposite beads after TC adsorption for solution contain 50 mg/L initial concentration of TC for 120 min at optimized pH 6 are presented. It turned out that the inhibition coefficient for tested microbial organisms after TC adsorption is increased compared to the values tested before adsorption (Fig. 2). The inhibition growth after adsorption followed the same order as in Fig. 2, yet with higher scores: *Bacillus subtilis* (100%) > *E. coli* (96%) > *Aspergillus fumigatus* (80%) > *Candida albicans* (76%).

3.4 Optimization of the adsorption by Box–Behnken design analysis

By means of analysis via Box–Behnken design, the adsorption process was optimized. We selected three variables of contact time (A), initial TC concentration (B), beads dose (C), with a temperature of 25℃. The dependence of the response, i.e. removal percentage Y, on these variables, was assumed to be quadratic, as described in Eq. 5 (see also Table S2):

$$Y_{TC} = 79 + 12.5A - 7B + 12.5C - 1.5AB + 3AC - 10.25A^2 - 3.25B^2 - 7.75C^2 \tag{5}$$

For assessing the statistical significance of the model, ANOVA was used. The quadratic model provided good fit, as shown by the high coefficient of determination R^2 (0.9827), see Table S3. It was determined that the quadratic
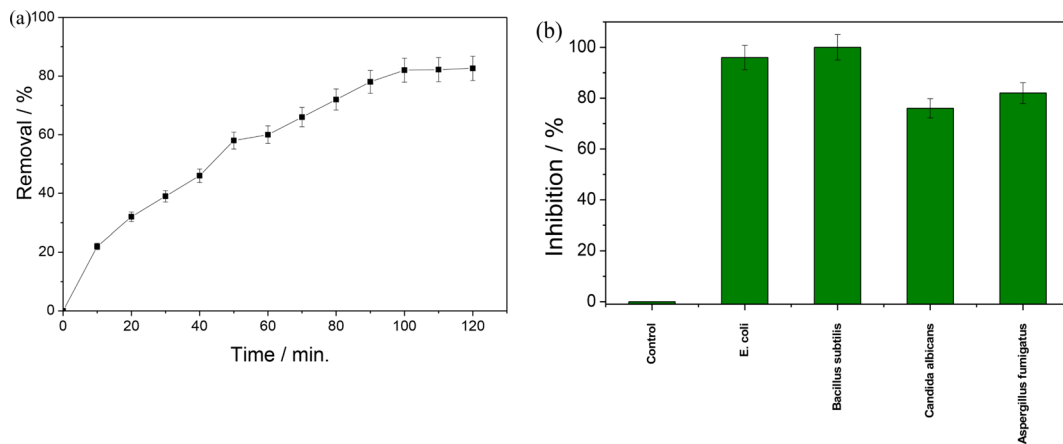
Fig. 4 (**a**) effect of contact time on TC adsorption, (**b**) confirmation test of the efficiency of TC adsorption on removal of different microbial organisms
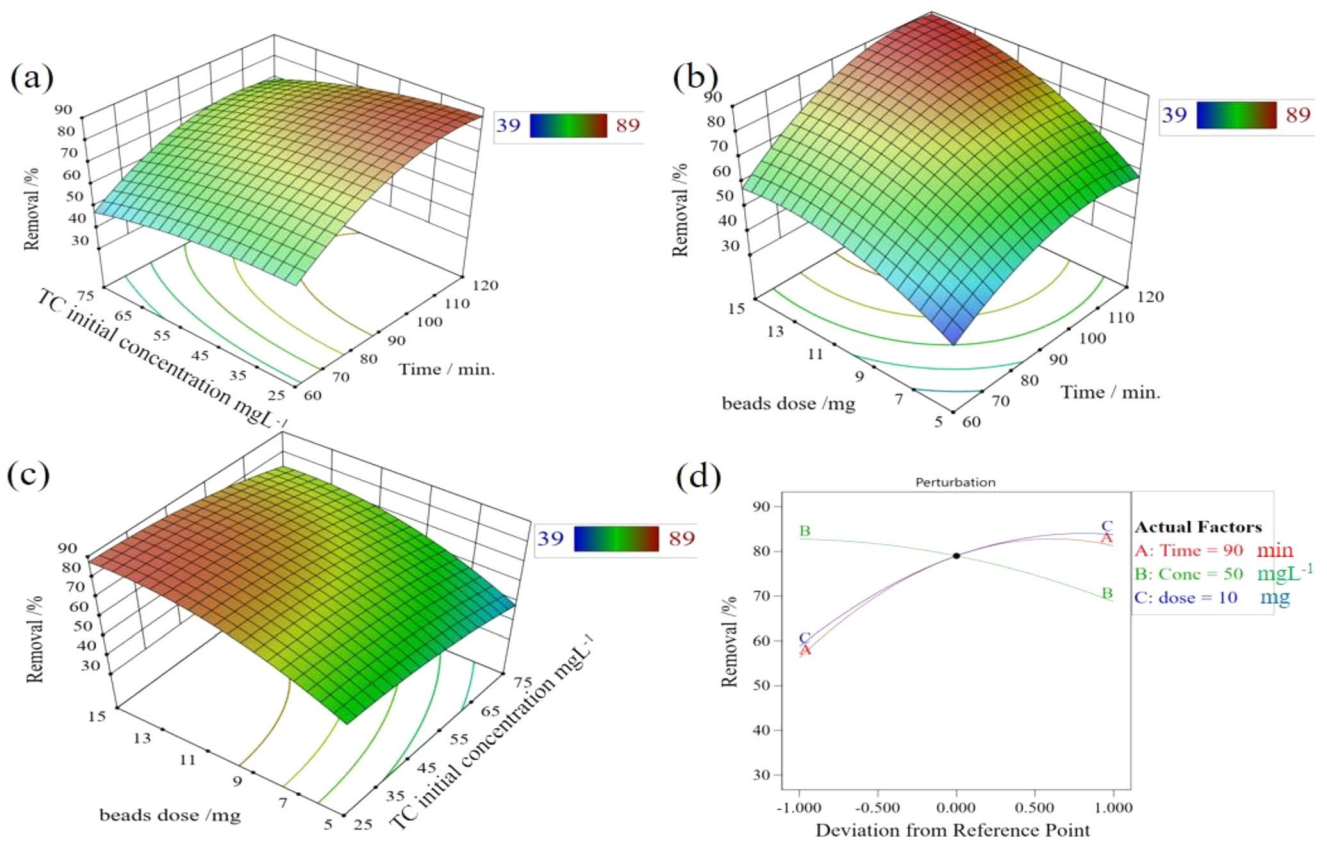

Fig. 5 3D surface plots of TC removal efficiency (%) of the prepared SGO_STiO$_2$@SA/CS/PVP nanocomposite beads

model was significant because the p value for TC removal efficiency was less than 0.0001. After our results, the following conditions emerged as the best possible: contact time 118 min, initial concentration 46 mg/L, beads 15 mg, which allow to achieve maximum removal of TC as high as 90.5%.

The 3D graphs presented in Fig. 5 illustrate the outcome of this analysis, and point out the interactions among the assessed variables. Apparently, the removal efficiency diminished with initial concentration increasing from 25 to 75 mg/L, while it raised when either the contact time or the beads dose was increased. Moreover, according to the perturbation plot shown in Fig. 5d, it was observed that time, TC initial concentration and beads dose significantly affect the removal efficiency. In particular, an increase in initial concentration of TC decreases the removal efficiency, while

an increase in either beads dose or adsorption time increases the removal efficiency.

3.5 Adsorption kinetics and isotherms

To better understand the adsorption for different initial concentrations of 50, 75, and 100 mg/L for TC on the prepared SGO_STiO$_2$@SA/CS/PVP nanocomposite beads, we set up pseudo-second-order kinetic models of the process. The data were fitted and the results are reported in Table 2 and Fig. S1. We compared the adsorption capacities resulting from the models with those ones found in the experiment. Whereas the pseudo-first-order model did not reproduce successfully the experimental values, the pseudo-second-order model produced values in good agreement with the experimental ones, with higher coefficients of determination (R^2). Because the adsorption obviously followed this pseudo-second-order model, chemisorption was the rate-limiting phase, and the accessibility of adsorption sites on the adsorbent surface determined the rate of adsorption for TC. The hydrogen bonds appear to result from chemical reactions or electron exchange between amino groups on TC and oxygenated groups on the nanocomposite beads [37]. Furthermore, the outcomes of the adsorption process's linear fitting align with the intraparticle diffusion model,

which divides the diffusion mechanism into three steps. First, the TC molecules are transported in the bulk solution; second, the TC charged molecules transfer into the pores and/or intraparticle active sites of the beads by either film diffusion of these solutes at the boundary layer or diffusion of charged molecules from bulk solution to the external surface of the beads; third, the TC charged molecules diffuse through the tiny pores of the beads and undergo a chemical binding reaction before reaching equilibrium.

Langmuir and Freundlich models were used at different temperatures and initial concentrations, as summarized in Table 2. One can see that the R^2 values of Langmuir model were quite near to 1, so this model represents well the adsorption data, which suggests that TC molecules adsorption is monolayer coverage, with a maximum q_m value of 357 mg/g appearing at high temperatures. However, the results of the Freundlich isotherm model also showed that the adsorption onto SGO_STiO$_2$@SA/CS/PVP nanocomposite beads was favorable. In contrast, it should be considered that the quantity $1/nF$, ranging from 0 to 1, represents an indicator of surface heterogeneity that is maximized when this value is close to zero. Consequently, we conclude that a heterogeneous chemisorption process took place, which is consistent with the kinetic model of intraparticle diffusion and the finding that TC molecules mostly adsorbed onto beads through the inner surface, which controls intraparticle diffusion.

3.6 Adsorption-desorption tests

Five adsorption–desorption cycles were conducted to assess the structural stability and reusability of our beads of SGO_STiO$_2$@SA/CS/PVP nanocomposite. Figure 6 shows that the removal efficiency remained high even after this repeated use, with just a negligible decline in removal coefficient following each desorption stage. This is encouraging for the potential application in large-scale industrial production of the nanocomposite beads for actual water filtration systems.

4 Conclusion

A novel type of nanocomposite beads for wastewater treatment was fabricated, resulting from polymer blending of sodium alginate (SA), chitosan (CS) and polyvinyl pyrrolidone (PVP) doped with sulfonated graphene oxide (SGO) and sulfonated titania (S-TiO$_2$). The prepared nanocomposite beads were tested for removal of tetracycline (TC) antibiotic residue from aqueous solutions. Following morphological and compositional characterization, it was found that the mechanism of adsorption is determined by

Table 2 Kinetics and isotherm models for TC adsorption process onto the prepared of SGO_STiO$_2$@SA/CS/PVP nanocomposite beads

TC Initial concentrations (mg/L)			
	50	75	100
$q_{e, exp}$ (mg/g)*	205	295	298
Pseudo-1st order			
$q_{e'cal}$ (mg/g)	851	346	850
k_1 (min^{-1})	0.065	0.022	0.051
R^2	0.772	0.972	0.741
Pseudo-2nd order			
$q_{e, cal}$ (mg/g)	246	333	357
k_2 (min^{-1})	0.004	0.003	0.0028
R^2	0.911	0.943	0.944
Intraparticle diffusion			
$k_{i,1}$	13.2	18.13	20.5
$k_{i,2}$	31.8	35.5	39.5
$k_{i,3}$	0.1	5.7	7.9
	Temperature ºC		
	25 ºC	35 ºC	45 ºC
Langmuir isotherm			
q_m (mg/g)	345	357	357
k_L (L/mg)	0.17	0.26	0.34
R^2	0.999	0.999	0.999
R_L	0.05	0.04	0.03
Freundlich isotherm			
K_F (mg/g)	115	145	159
$1/n_F$	0.27	0.22	0.21
R^2	0.997	0.994	0.997

Fig. 6 Adsorption–desorption cycles of TC in SGO_STiO$_2$@SA/CS/PVP nanocomposite beads of 0.01 g amount, with 20 mg/L initial concentration, pH 6 and 25 °C temperature
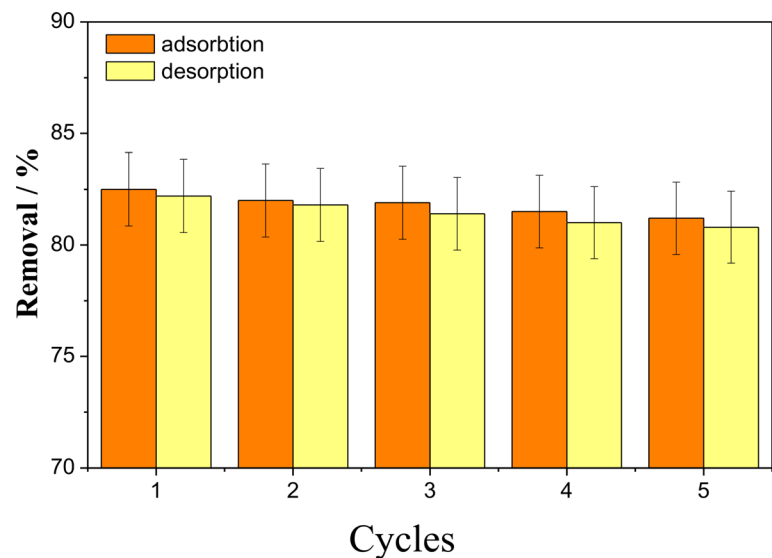
the functional groups of the TC molecules interacting with the various functional groups of the composite beads. The biocidal action of the nanocomposite beads against different microbial organisms was tested and the results showed good antibacterial activities at standard concentration. We used the response surface methodology design to find the conditions for best removal efficiency of TC, achieving values as high as 90.5%; the best conditions were: contact time 118 min, initial concentration 46 mg/L, nanocomposite beads 15 mg. The analysis of SGO_STiO$_2$@SA/CS/PVP nanocomposite beads absorbance using kinetic models allowed us to better understand the removal mechanism, which appeared to combine electrostatic adsorption and chemisorption by the functional groups in the beads and TC molecules. We also demonstrated reusability, by repeating five absorption-desorption cycles. This study shows that, to meet the objectives of waste management and wastewater treatment, waste-derived materials can be used based on the "wastes-treat-wastes" approach.

Author contributions N. M. requested the fund and project management, M. H. G. performed the investigation and wrote the first draft, M. A. helped in project management, M.S. tabulated the results and produced the figures and wrote the first draft, A. M. A. revised the first draft, N. A. E. design and supervise the work, reviewed & edited the final version and submitted the manuscript. All authors reviewed the manuscript.

Data availability No datasets were generated or analysed during the current study.

Declarations

Ethical approval Not applicable. The research did not involve human participants or animals.

Consent to participate Not applicable.

Consent to publish Not applicable.

Competing interests The authors declare no competing interests.

References

1. Yang, Y., Song, W., Lin, H., Wang, W., Du, L., Xing, W.: 'Antibiotics and antibiotic resistance genes in global lakes: A review and meta-analysis', Environment International, vol. 116. Elsevier Ltd, pp. 60–73, Jul. 01, (2018). https://doi.org/10.1016/j.envint.2018.04.011

2. Yue, Y., Shen, C., Ge, Y.: Biochar accelerates the removal of tetracyclines and their intermediates by altering soil properties. J. Hazard. Mater. **380** (Dec. 2019). https://doi.org/10.1016/j.jhazmat.2019.120821

3. Santás-Miguel, V., et al.: Mar., 'Interactions between soil properties and tetracycline toxicity affecting to bacterial community growth in agricultural soil', Applied Soil Ecology, vol. 147, (2020). https://doi.org/10.1016/j.apsoil.2019.103437

4. Xu, L., Zhang, H., Xiong, P., Zhu, Q., Liao, C., Jiang, G.: 'Occurrence, fate, and risk assessment of typical tetracycline antibiotics in the aquatic environment: A review', Science of the Total Environment, vol. 753. Elsevier B.V., Jan. 20, (2021). https://doi.org/10.1016/j.scitotenv.2020.141975

5. Li, Z., Wang, X., Xu, N., Xiao, Y., Ma, L., Duan, J.: Cost-effective and visible-light-driven melamine-derived sponge for tetracyclines degradation and Salmonella inactivation in water. Chem. Eng. J. **394** (Aug. 2020). https://doi.org/10.1016/j.cej.2020.124913

6. Mohy Eldin, M.S., Gouda, M.H., Youssef, M.E., El-Shazly, Y.M.S., Farag, H.A.: 'Removal of methylene blue by amidoxime polyacrylonitrile-grafted cotton fabrics: Kinetic, equilibrium, and simulation studies', Fibers and Polymers, vol. 17,

no. 11, pp. 1884–1897, Nov. (2016). https://doi.org/10.1007/s12221-016-6373-3

7. Mohy Eldin, M.S., Gouda, M.H., Abu-Saied, M.A., El-Shazly, Y.M.S., Farag, H.A.: Development of grafted cotton fabrics ions exchanger for dye removal applications: Methylene blue model. Desalin. Water Treat. **57**(46), 22049–22060 (Oct. 2016). https://doi.org/10.1080/19443994.2015.1128363

8. Elessawy, N.A., et al.: Jan., 'Ciprofloxacin removal using magnetic fullerene nanocomposite obtained from sustainable PET bottle wastes: Adsorption process optimization, kinetics, isotherm, regeneration and recycling studies', Chemosphere, vol. 239, (2020). https://doi.org/10.1016/j.chemosphere.2019.124728

9. Zhang, W., et al.: Nov., 'A facile synthesis of core-shell/bead-like poly (vinyl alcohol)/alginate@PAM with good adsorption capacity, high adaptability and stability towards Cu(II) removal', Chemical Engineering Journal, vol. 351, pp. 462–472, (2018). https://doi.org/10.1016/j.cej.2018.06.129

10. Lucaci, A.R., Bulgariu, D., Ahmad, I., Bulgariu, L.: 'Equilibrium and kinetics studies of metal ions biosorption on alginate extracted from marine red algae biomass (Callithamnion corymbosum sp.)', Polymers (Basel), vol. 12, no. 9, Sep. (2020). https://doi.org/10.3390/POLYM12091888

11. Luo, H., et al.: Phosphorus removal and recovery from water with macroporous bead adsorbent constituted of alginate-Zr4 + and PNIPAM-interpenetrated networks. Int. J. Biol. Macromol. **126**, 1133–1144 (Apr. 2019). https://doi.org/10.1016/j.ijbiomac.2018.12.269

12. Luo, H., Rong, H., Zhang, T.C., Zeng, X., Wan, J.: Amino-functionalized magnetic zirconium alginate beads for phosphate removal and recovery from aqueous solutions. J. Appl. Polym. Sci. **136**(1) (Jan. 2019). https://doi.org/10.1002/app.46897

13. Luo, H., Liu, Y., Lu, H., Fang, Q., Rong, H.: 'Efficient Adsorption of Tetracycline from Aqueous Solutions by Modified Alginate Beads after the Removal of Cu(II) Ions', ACS Omega, vol. 6, no. 9, pp. 6240–6251, Mar. (2021). https://doi.org/10.1021/acsomega.0c05807

14. Sabe, M.M., et al.: 'Effect of tween 20 as plasticizer on cinnamyl chitosan membranes: Preparation, characterization and antimicrobial evaluation', Egyptian Journal of Chemistry, vol. 63, no. 6. NIDOC (Nat.Inform.Document.Centre), pp. 1989–1998, Jun. 01, (2020). https://doi.org/10.21608/ejchem.2019.6679.1561

15. Erdem, S., Öztekin, M., Sağ Açıkel, Y.: Investigation of tetracycline removal from aqueous solutions using halloysite/chitosan nanocomposites and halloysite nanotubes/alginate hydrogel beads. Environ. Nanotechnol Monit. Manag. **16** (Dec. 2021). https://doi.org/10.1016/j.enmm.2021.100576

16. Toghan, A., Gouda, M.H., Zahran, H.F., Alakhras, A.I., Sanad, M.M.S., Elessawy, N.A.: Development of a new promising nanocomposite photocatalyst of polyaniline/carboxylated graphene oxide supported on PVA film to remove different ecological pollutants. Diam. Relat. Mater. **139** (Nov. 2023). https://doi.org/10.1016/j.diamond.2023.110400

17. Tian, F., Wu, Z., Chen, Q., Yan, Y., Cravotto, G., Wu, Z.: 'Microwave-induced crystallization of AC/TiO 2 for improving the performance of rhodamine B dye degradation', Appl Surf Sci, vol. 351, pp. 104–112, Oct. (2015). https://doi.org/10.1016/j.apsusc.2015.05.133

18. Elessawy, N.A., et al.: Oct., 'Novel sodium alginate/polyvinyl-pyrrolidone/tio2 nanocomposite for efficient removal of cationic dye from aqueous solution', Applied Sciences (Switzerland), vol. 11, no. 19, (2021). https://doi.org/10.3390/app11199186

19. Dikin, D.A., et al.: Jul., 'Preparation and characterization of graphene oxide paper', Nature, vol. 448, no. 7152, pp. 457–460, (2007). https://doi.org/10.1038/nature06016

20. Dong, Z., Wang, D., Liu, X., Pei, X., Chen, L., Jin, J.: Bio-inspired surface-functionalization of graphene oxide for the adsorption of organic dyes and heavy metal ions with a superhigh capacity. J. Mater. Chem. Mater. **2**, 5034–5040 (Apr. 2014). https://doi.org/10.1039/c3ta14751g

21. Elessawy, N.A., Gouda, M.H., Elkady, M.F., Ali, S.M., Gouda, M., Mohy Eldin, M.S.: 'Ultra-fast removal of cadmium and lead from wastewater using high-efficient adsorbent derived from plastic waste: Statistical modeling kinetic and isotherm studies', Desalination Water Treat, vol. 173, pp. 394–408, Jan. (2020). https://doi.org/10.5004/dwt.2020.24809

22. Elessawy, N.A., Gouda, M.H., Ali, S.M., Salerno, M., Eldin, M.S.M.: 'Effective elimination of contaminant antibiotics using high-surface-area magnetic-functionalized graphene nanocomposites developed from plastic waste', Materials, vol. 13, no. 7, Apr. (2020). https://doi.org/10.3390/ma13071517

23. Elessawy, N.A., Gouda, M.H., Elnouby, M., Ali, S.M., Salerno, M., Youssef, M.E.: 'Sustainable Microbial and Heavy Metal Reduction in Water Purification Systems Based on PVA/IC Nanofiber Membrane Doped with PANI/GO', Polymers (Basel), vol. 14, no. 8, Apr. (2022). https://doi.org/10.3390/polym14081558

24. Zhao, G., et al.: Sep., 'Sulfonated graphene for persistent aromatic pollutant management', Advanced Materials, vol. 23, no. 34, pp. 3959–3963, (2011). https://doi.org/10.1002/adma.201101007

25. Dreyer, D.R., Park, S., Bielawski, C.W., Ruoff, R.S.: The chemistry of graphene oxide. Chem. Soc. Rev. **39**, 228–240 (Jan. 2010). https://doi.org/10.1039/b917103g

26. Gouda, M.H., Konsowa, A.H., Farag, H.A., Elessawy, N.A., Tamer, T.M.: Mohy Eldin, 'Novel nanocomposite membranes based on cross-linked eco-friendly polymers doped with sulfated titania nanotubes for direct methanol fuel cell application'. Nanomaterials Nanatechnol. **10** (2020). https://doi.org/10.1177/1847980420964368

27. Box, G.E.P., Behnken, D.W.: 'American Society for Quality Some New Three Level Designs for the Study of Quantitative Variables', (1960)

28. Gouda, M.H., et al.: Aug., 'Evaluation of sulfonated chitosan-g-sulfonated polyvinyl alcohol/polyethylene oxide/sulfated zirconia composite polyelectrolyte membranes for direct borohydride fuel cells: Solution casting against the electrospun membrane fabrication technique', Front Mater, vol. 9, (2022). https://doi.org/10.3389/fmats.2022.912006

29. Elessawy, N.A., Toghan, A., Elnouby, M.S., Alakhras, A.I., Hamad, H.A., Youssef, M.E.: 'Development and activity enhancement of zirconium/vanadium oxides as micro-heterogeneous ceramic electrocatalyst for ORR in low temperature fuel cell', Ceram Int, vol. 49, no. 3, pp. 4313–4321, Feb. (2023). https://doi.org/10.1016/j.ceramint.2022.09.316

30. Gouda, M.H., et al.: Poly(vinyl alcohol)-based crosslinked ternary polymer blend doped with sulfonated graphene oxide as a sustainable composite membrane for direct borohydride fuel cells. J. Power Sources. **432**, 92–101 (Aug. 2019). https://doi.org/10.1016/j.jpowsour.2019.05.078

31. Gouda, M.H., Elessawy, N.A., Santos, D.M.F.: 'Synthesis and characterization of novel green hybrid nanocomposites for application as proton exchange membranes in direct borohydride fuel cells', Energies (Basel), vol. 13, no. 5, Mar. (2020). https://doi.org/10.3390/en13051180

32. Jun, B.M., Heo, J., Taheri-Qazvini, N., Park, C.M., Yoon, Y.: 'Adsorption of selected dyes on Ti3C2Tx MXene and Al-based metal-organic framework', Ceram Int, vol. 46, no. 3, pp. 2960–2968, Feb. (2020). https://doi.org/10.1016/j.ceramint.2019.09.293

33. Gurunathan, S., Kim, J.H.: 'Synthesis, toxicity, biocompatibility, and biomedical applications of graphene and graphene-related materials', International Journal of Nanomedicine, vol. 11. Dove Medical Press Ltd., pp. 1927–1945, May 05, (2016). https://doi.org/10.2147/IJN.S105264

34. Kumar, P., Huo, P., Zhang, R., Liu, B.: Antibacterial Properties of graphene-based Nanomaterials', Nanomaterials, vol. 9, 5no. edn. MDPI AG, May 01, (2019). https://doi.org/10.3390/nano9050737

35. Younis, A.B., et al.: Synthesis and characterization of TiO2 nanoparticles combined with geraniol and their synergistic antibacterial activity. BMC Microbiol. **23**(1) (Dec. 2023). https://doi.org/10.1186/s12866-023-02955-1

36. Guo, Z., et al.: Jul., 'Removal of tetracycline from water using activated carbon derived from the mixture of phragmites australis and waterworks sludge', ACS Omega, vol. 5, no. 26, pp. 16045–16052, (2020). https://doi.org/10.1021/acsomega.0c01524

37. Ahmed, I., Hasan, Z., Lee, G., Lee, H.J., Jhung, S.H.: 'Contribution of hydrogen bonding to liquid-phase adsorptive removal of hazardous organics with metal-organic framework-based materials', Chemical Engineering Journal, vol. 430, Feb. (2022). https://doi.org/10.1016/j.cej.2021.132596